applied sciences

MDPI

Article

Seismic Sedimentology for the Characterization of Quaternary Evaporite Facies in Biogas-Bearing Taidong Area, Sanhu Depression, Qaidam Basin, NW China

Guoyong Liu [1,2], Zhaohui Xu [1,2,3,*], Jiangtao Li [1,2], Yong Song [3], Hongliu Zeng [4], Xiaomin Zhu [5], Jixian Tian [3], Chunming Lin [6] and Lei Jiang [7]

[1] PetroChina Qinghai Oilfield Company, Dunhuang 736202, China; liuguoyong@petrochina.com.cn (G.L.); ljtqh@petrochina.com.cn (J.L.)
[2] Qinghai Provincial Key Laboratory of Plateau Saline-Lacustrine Basinal Oil & Gas Geology, Dunhuang 736202, China
[3] PetroChina Research Institute of Petroleum Exploration & Development, Beijing 100083, China; syong@petrochina.com.cn (Y.S.); tjx69@petrochina.com.cn (J.T.)
[4] Bureau of Economic Geology, Jackson School of Geosciences, The University of Texas at Austin, Austin, TX 78712, USA; hongliu.zeng@beg.utexas.edu
[5] College of Geosciences, China University of Petroleum, Beijing 102249, China; xmzhu@cup.edu.cn
[6] State Key Laboratory for Mineral Deposits Research, School of Earth Sciences and Engineering, Nanjing University, Nanjing 210046, China; cmlin@nju.edu.cn
[7] State Key Laboratory of Lithospheric and Environmental Coevolution, Institute of Geology and Geophysics, Chinese Academy of Sciences, Beijing 100029, China; lei.jiang@mail.iggcas.ac.cn
* Correspondence: tadxu@126.com; Tel.: +86-1083599233

Abstract: S-wave seismic data are unaffected by natural gas trapped in strata, making them a valuable tool to study evaporite facies comparing to P-wave data. S-wave seismic data were utilized to construct an isochronous framework and analyze evaporite facies by seismic sedimentology methods in the Quaternary biogenic gas-bearing Taidong area, Sanhu Depression, Qaidam Basin, NW China, with calibration from wireline logs, geochemical evidences, and modern analogs. Techniques of phase rotation, frequency decomposition, R (Red), G (Green), B (Blue) fusion, and stratal slices were integrated to reconstruct seismic geomorphological features. Linear and sub-circular morphologies, resembling those observed in modern saline pans such as Lake Chad, were identified. Observations from Upper Pleistocene outcrops of anhydrite and halite at Yanshan (east of the Taidong area), along with lithological and paleo-environmental records from boreholes SG-5, SG-1, and SG-1b (northwest of the Taidong area), support the seismic findings. The slices generated from the S-wave seismic data indicate a progressive increase in the occurrence of evaporite features from the K2 standard zone upwards. The vertical occurrence of evaporite facies in the Taidong area increases, which coincides with the contemporary regional and global arid paleo-environmental changes. The interpretation of Quaternary stratal slices reveals a transition from a freshwater lake to brackish, saline, and finally, a dry saline pan, overlaid by silt. This analysis provides valuable insights into locating evaporites as cap rocks for biogenic gas accumulation and also into mining the evaporite mineral resources in shallow layers of the Taidong area.

Keywords: seismic sedimentology; seismic geomorphology; Quaternary evaporite facies; S-wave 3D seismic data; evaporite minerals; biogenic gas reservoirs; subsurface fluid migration; Taidong area; Sanhu Depression; Qaidam Basin

Academic Editor: Tiago Filipe da Silva Miranda

Received: 2 January 2025
Revised: 17 February 2025
Accepted: 18 February 2025
Published: 20 February 2025

Citation: Liu, G.; Xu, Z.; Li, J.; Song, Y.; Zeng, H.; Zhu, X.; Tian, J.; Lin, C.; Jiang, L. Seismic Sedimentology for the Characterization of Quaternary Evaporite Facies in Biogas-Bearing Taidong Area, Sanhu Depression, Qaidam Basin, NW China. *Appl. Sci.* **2025**, *15*, 2288. https://doi.org/10.3390/app15052288

1. Introduction

Biogenic gas, characterized by its high methane content, represents a more environmentally friendly energy source compared to oil, coal, and other fossil fuels. It has been discovered in several basins worldwide, including the Cook Inlet Basin in Alaska [1], the West Siberian Basin in Russia [2], the Central Pannonian Basin in Hungary [3], and the North Papua Basin in Indonesia [4]. Over 20% of global gas reserves are of biogenic origin [5], with several giant biogenic gas fields, such as Agostino-Porto Garibaldi in Italy [3.5 trillion cubic feet (Tcf) original gas in place], Sebei-1 in the Sanhu Depression (China, 95 Tcf), and Urengoy in Russia (220 Tcf) [3]. Due to its "green energy" attributes, widespread distribution, and shallow burial depth, biogenic gas is becoming an increasingly important resource. In the Sanhu Depression, Qaidam Basin, NW China, biogenic gas has been produced continuously for 13 years, with an annual output of 0.18 Tcf [6].

The primary moderate-buried (1000–1500 m) gas-bearing zones in the Sanhu Depression are sealed by mudrock rather than hydrostatic pressure [5,7]. However, compared to mudrock and hydrostatic pressure, halite possesses superior sealing capacity. In the Sanhu Depression, where loose sediments are prevalent, the presence of an effective sealing cap rock is a key factor controlling biogenic gas accumulation. Evidence from outcrops and groundwater tests reveals the presence of evaporite lithologies, such as halite and anhydrite, in shallow layers (less than 800 m) in the region. The global decline in temperature and precipitation since the Late Quaternary aligns with the evaporite environment observed in the Qaidam Basin [8,9]. Numerous wells have confirmed the presence of biogenic gas in shallow layers, ranging from tens to several hundred meters in depth, likely sealed by evaporites. The distribution of evaporites, particularly halite and anhydrite, has become a critical issue for biogenic gas exploration and development as well as for evaporites mining in the Sanhu Depression. However, due to the influence of gas chimney or gas cloud, traditional P-wave seismic data cannot be used to set up stratal framework, let alone to predict lithology distribution.

Halite may precipitate in restricted areas such as marine basins, inland seas, nonmarine brine lakes, and salt pans [10,11]. Salt pans have been investigated primarily through outcrops, satellite images, and modern sediment studies [12,13]. Seismic and well data are proved to be effective to quantitatively investigate evaporite sequence [14]. However, few studies have utilized S-wave 3D seismic data [15], which has superior vertical resolution than P-wave data in shallow layers to investigate evaporite facies (i.e., distribution of evaporite environment and evaporite lithologies) because of the lacking of S-wave data.

Taidong area is located in the northwest of Sanhu Depression, and is covered by a newly acquired S-wave 3D seismic data. Considering the superior vertical resolution of S-wave seismic data and the decent lateral resolution of stratal slices (e.g., a meandering channel is tens of meters deep that is beyond of seismic vertical resolution; but several kilometers long that can be interpreted easily on slices), this paper applies seismic sedimentology to the S-wave 3D seismic data, revealing unique sub-circular features on RGB-fused slices generated from the Quaternary strata in the Taidong area, west of the Sebei-1 gas field, for the first time. Considering the geological context and modern analogs, these features are interpreted as saline pans [16], formed in continental lacustrine and eolian interdunal playa environments [17]. The morphological and structural features observed in the geophysical (seismic) data, combined with geochemical evidence (salinity data), confirm the existence and evolution of salt pans in the area. The insights gained from this paper are valuable not only for theoretical research on Quaternary environments but also for practical applications in the exploration and development of biogenic gas. Moreover, the distribution and evolution of evaporite facies in the Taidong area may assist in the mining of evaporite resources.

2. Geological Setting

The Qaidam Basin, located on the northeastern Tibetan Plateau, is an intermontane basin surrounded by the Altun, Qilian, and Kunlun Mountains (Figure 1a). The average elevations of the basin and the surrounding mountains are 2800 m and 4000–5000 m, respectively [18]. Covering an area of 12×10^4 km^2, the basin is situated on Proterozoic crystalline and Paleozoic folded basements. Its tectonic evolution has occurred in four distinct stages: rifting from the Early to Middle Jurassic, compression from the Late Jurassic to Cretaceous, local strike-slip and regional compression from the Paleogene to Late Pliocene, and compressional folding and depression from the Late Pliocene to the Quaternary [19]. The basin's evolution provides important insights into the tectonic processes of the Tibetan Plateau, and the plateau has influenced Quaternary climate of the Northern Hemisphere [20].

In the Sanhu Depression of the Qaidam Basin, tectonic activity and the Quaternary drying climate have resulted in thick sediment accumulation during the Pleistocene and Holocene [21]. Sediments deposited since 2.8 Ma BP are divided into standard zones from K13 to K0″ upward. The Pleistocene is further divided into three subunits: Lower Pleistocene [Q1, K13 (2.8 Ma BP) to K0 (0.73 Ma BP)], Middle Pleistocene [Q2, K0 (0.73 Ma BP) to K0′ (0.12 Ma BP)], and Upper Pleistocene [Q3, K0′ (0.12 Ma BP) to K0″ (0.01 Ma BP)]. The Holocene corresponds to Q4 [K0″ (0.01 Ma BP) to the present]. Drilling in the Sanhu Depression has revealed over 3000 m of Quaternary mudrock, carbonaceous dark grey mudrock, grey siltstone, and greyish-green argillaceous siltstone, with evaporites (i.e., anhydrite and halite) present in shallow zones and at the surface (Figure 1b). The lithologies are lose and weak diagenetic. Water parameters indicate the strengthened sealing ability in Qigequan Formation [22]. During the formation of the sediments in the Taidong area, northwestern of Sanhu Depression and western of Sebei-1 gas field, the lake level was shallow in the K13 to K10 (delta front facies) and K5 to K3 (delta front to prodelta facies) intervals, while it was deep in the K9 to K6 (lacustrine facies) and shallow K2 to K0 (lagoon to salt pan facies) intervals. The last period of shallow lake levels coincided with the emergence of an evaporite lagoon at west part of Taidong area [6]. The evolution of sedimentary facies and lithologies from K13 to K0, particularly the presence of halite in K0′ (Upper Pleistocene) and K0″ (Holocene), reflects the extreme arid conditions that characterize the region, in line with the regional climate changes in the Qaidam Basin [23]. The change of water level and climate may influence the sedimentary facies in Taidong area.

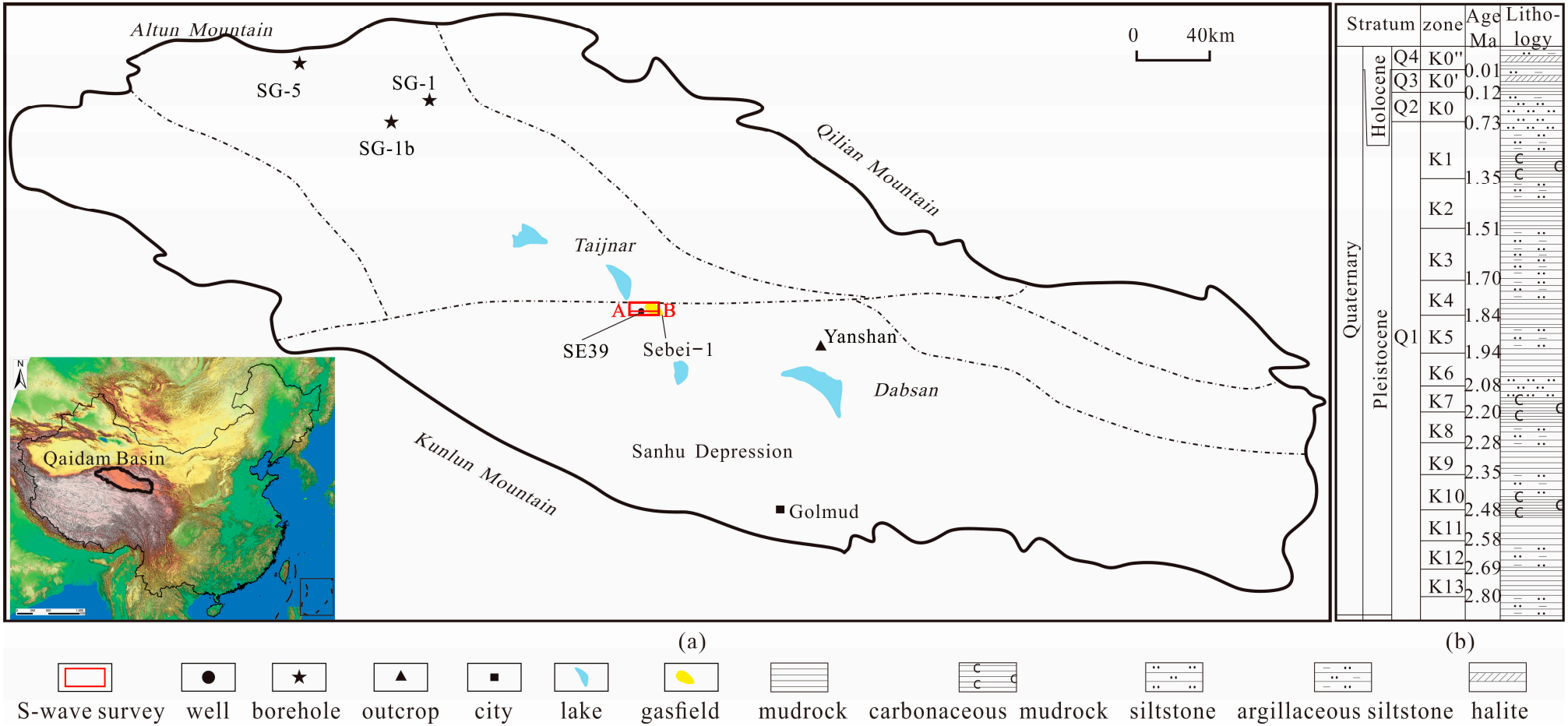

Figure 1. Location of Qaidam Basin, data points in the basin (**a**), and Quaternary lithological column in Sanhu Depression (**b**).

3. Data and Methods

This section provides an overview on data, e.g., geophysical, geochemical, and geological and methods i.e., seismic sedimentological that used in this paper.

3.1. Data

This paper utilizes seismic, wireline log, drill core, outcrop, and related geochemical test data. The 82.5 km^2 Taidong S-wave 3D seismic dataset, acquired west of the Sebei-1 gas field in the Taidong area, is not influenced by biogenic gas in the strata (Figure 2). The seismic survey was acquired by EV56S shear-wave vibrator and processed into fast and slow S-wave data [15]. The survey has a bin spacing of 20 m in the inline direction and 10 m in the crossline direction, with a time sampling rate of 2 milliseconds. The predominant frequency varies across different strata: 26 Hz from K13 to K10, 25 Hz from K9 to K6, 33 Hz from K5 to K3, 18 Hz from K2 to K0, and 31 Hz from K0 to K0″. Well SE39, which includes S-wave acoustic wireline logs (DTS) and density logs (DEN), was used for tying the well data to the S-wave 3D seismic data. A decent well-seismic tie shows that the average interval velocity from K13 to K0′ is 2917 m/s to 801 m/s for P-wave data and 1406 m/s to 343 m/s for S-wave data. As a result, the S-wave 3D seismic data offer better vertical resolution (3~13 m, 28 Hz) compared to P-wave data (7~24 m, 30 Hz) from K13 upward, particularly in the shallower standard zones for their low velocity.

Geochemical data from boreholes SG-1, SG-1b, and SG-5 in the western part of the Qaidam Basin were referenced and analyzed from published literature to interpret the evolution of paleoclimate from a geochemical perspective. The modern evaporitic analog from northeast Lake Chad, a present key to the past, was used as a geological model to analyze Quaternary sedimentary facies in the Taidong area.

3.2. Methods

Seismic sedimentology, a concept developed after sequence stratigraphy, is employed to study sedimentary rocks and depositional processes using seismic data [24,25]. Seismic sedimentology incorporates two complementary aspects: model-driven seismic geomorphology and data-driven seismic lithology [26]. An integrated seismic sedimentological workflow was developed by integrating geophysical, geochemical (elements and isotopes), and geological data to reconstruct evaporite facies in the Taidong area (Figure 3). The S-wave 3D seismic dataset was first phase-rotated to -90° to make the seismic event corresponding to stratum. Wireline logs, including DTS and DEN, were then used to tie the phase-rotated seismic data. After achieving a good well-seismic tie, boundaries of the standard zones were interpreted. These boundaries define an isochronous framework, providing a connection between the two-way travel time in the seismic data and the depth and geological age indicated by the standard zones (Figures 1 and 3). This connection is essential for analyzing the relationship between sedimentary facies and regional climate change.

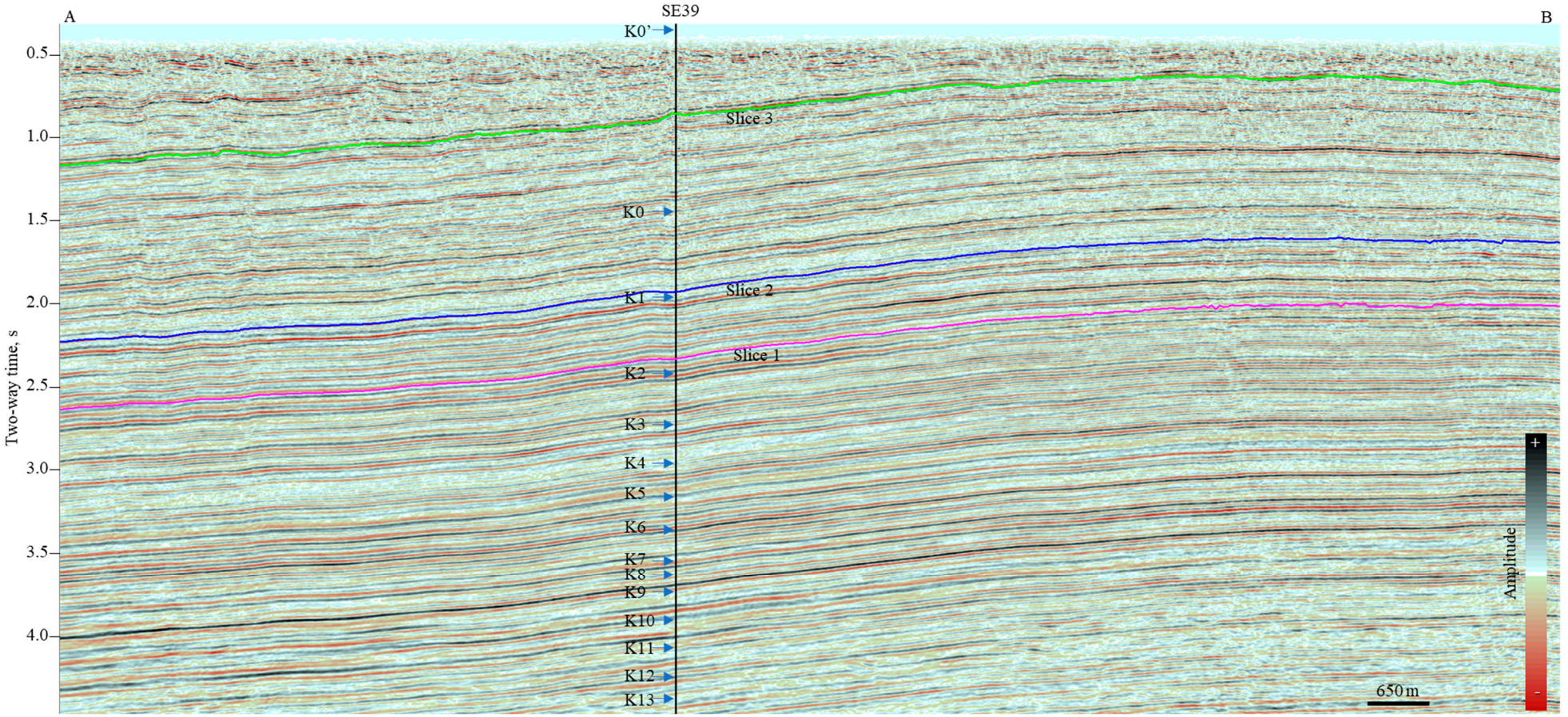

Figure 2. A S-wave 3D seismic profile (L130) crossing Well SE39 in Taidong area, Sanhu Depression, Qaidam Basin (see the location of profile A-B in Figure 1).

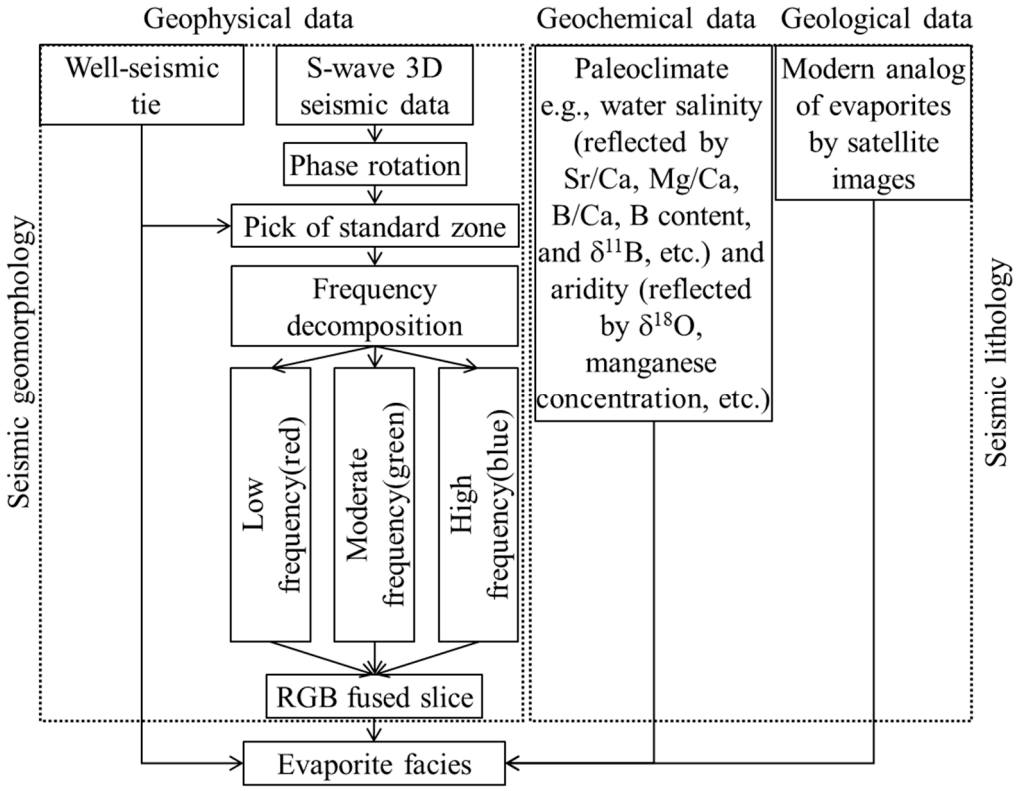

Figure 3. Data and workflow used in this paper.

Average frequency and interval velocity of the studied K2 to K0′ is 25 Hz and 600 m/s, respectively. Then the S-wave seismic data with predominant frequency of 25 Hz have a vertical resolution of 6 m according to a quarter of λ [27]. Considering the seismic frequency bandwidth and stratum thickness in Taidong area, the low and high frequency is determined to be 7 Hz (21 m resolution) and 35 Hz (4 m resolution). The phase-rotated seismic data were decomposed into three sub-cubes using a wavelet algorithm: low-frequency (7 Hz), moderate-frequency (25 Hz), and high-frequency (35 Hz) components. These sub-cubes were then fused using the RGB method, where red, green, and blue represent low, moderate, and high frequencies, respectively. In this scheme, low frequencies correspond to thicker strata, moderate frequencies indicate intermediate thickness, and high frequencies reflect thinner layers (Xu et al., 2024). The independent nature of the three primary colors in the RGB fusion allows for the expression of geological features at different scales simultaneous [28,29]. Stratal slices were generated from the RGB-fused cube and subsequently interpreted according to the geomorphology features and information derived from geochemical and geological data.

The geochemical data, i.e., element and isotopes derived from regional (boreholes SG-1, SG-1b, and SG-5) and global (temperature anomaly in the Equatorial West Pacific and precipitation anomaly in China and East Asian) parameters, reflect variables such as precipitation, temperature, and water salinity. Geological data, including modern Lake Chad's evaporite environment and published saline pan models, were used for further interpretation. Stratal slices were generated every two milliseconds, corresponding to the sampling rate of the S-wave seismic data, starting from the bottom of K2 (1.5 Ma BP) upwards. The slices reveal clear lateral geomorphology features with different scales, which is the key to interpret evaporite facies in Taidong area. Three representative slices (Slice 1, 2, and 3) from the K2, K1, and K0 standard zones, where aridity and water salinity are different (Figure 2) were selected to investigate seismic facies by seismic geomorphology and seismic lithology. These seismic facies were then transformed into sedimentary facies

by integrating geochemical and geological information in Qaidam Basin and modern analogs in Lake Chad. Time-structural maps of the three slices assisted in interpreting the sedimentary environments in Taidong area.

4. Results

Stratal slices were generated by seismic geomorphology and show us an outlook of the morphology features. According to quantitative reginal geochemical, mineral, and lithological data, evaporite facies were analyzed by seismic lithology.

Slice 1 (Figure 4) exhibits two distinct regions: the eastern part (T960 to T1720), characterized by red to pink hues, and the western part (T200 to T960), where green to yellow colors dominate. The color variations indicate differing strata thickness, with the eastern part being thicker than the western. The strong color contrast between red and blue in the eastern region (L40 to L300, II) suggests high heterogeneity, while the weak contrast in the western region (I) reflects relatively low heterogeneity. In the eastern section (II), linear blue morphologies orienting NNE-SSW or NNE-SSE are visible, some of which are interconnected (e.g., at the point L240, T1360). In the western section (I), concentric bands of green to yellow surround the eastern area.

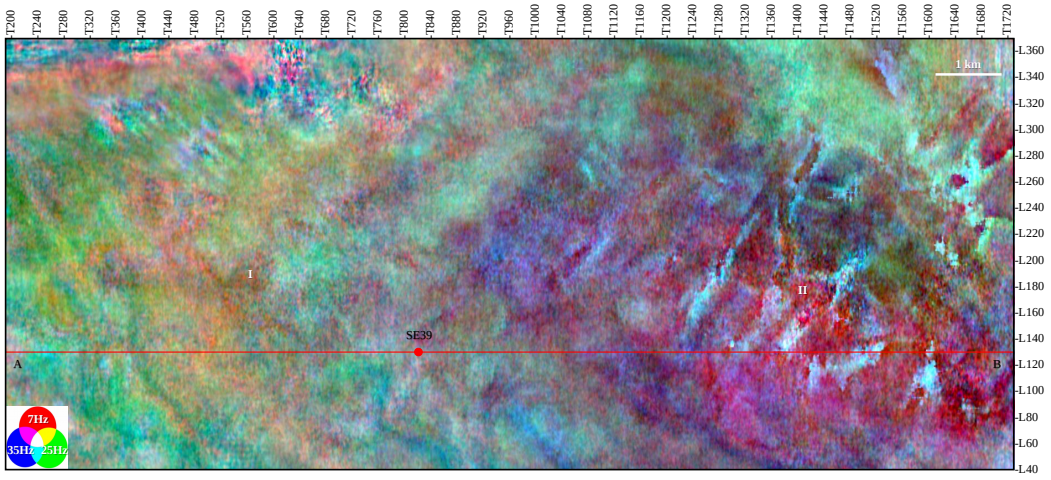

Figure 4. RGB-fused stratal slice 1 at lower K2 in Taidong area, Sanhu Depression, Qaidam Basin (see the pink line for the slice location in Figure 2). A-B shows the location of the L130. Letters I and II show the locations discussed in the text.

On the RGB-fused stratal slice 2 (Figure 5), the eastern region is predominantly green (T960 to T1720, III), while the western region (T200 to T960) transitions from red (I) to pink (II). This color distribution indicates that the western part is thicker than the eastern. The linear morphologies observed in slice 1 evolve into sub-circular polygons that extend further to the west and north. At the boundaries of the sub-circular polygons (III-1), the colors transition from blue to purple, while the interiors (III-2) range from green to yellow. These observations suggest a distinct vertical frequency structure of the polygons, with higher frequency at the boundaries and lower frequency within the interiors. The average diameter of these polygons is approximately 1 km.

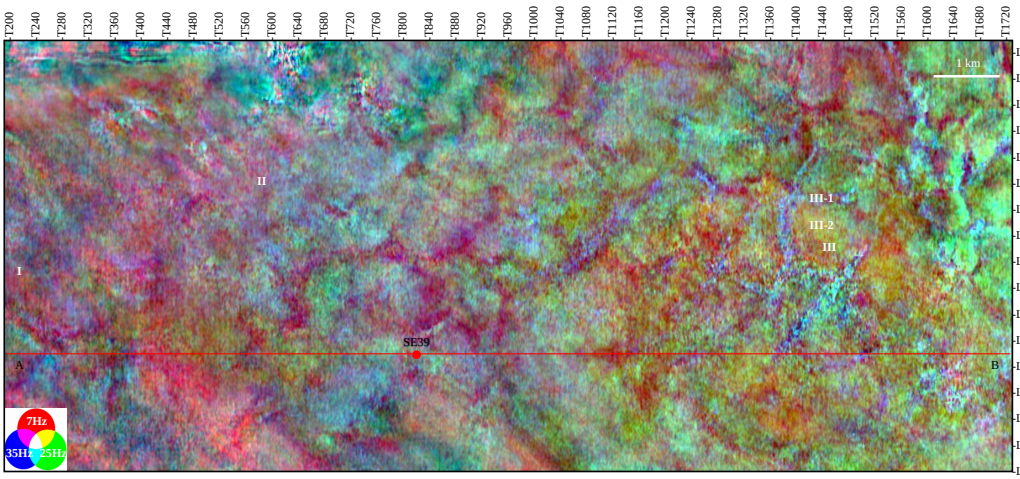

Figure 5. RGB-fused stratal slice 2 at lower K1 in Taidong area, Sanhu Depression, Qaidam Basin (see the blue line for the slice location in Figure 2). A-B shows the location of the L130. Letters I, II, III, III-1, and III-2 show the locations discussed in the text.

The RGB-fused stratal slice 3 (Figure 6), generated from the middle of K0 standard zone, shows a relatively thin (green to yellow) feature in the study area. The sub-circular morphologies extend further from the eastern location (III), where these morphologies initially appear, they are replaced by a larger elliptical feature (L40 to L260, T1040 to T1720, III-1). The diameter of the larger ellipse is approximately 6.5 km. The boundaries (III-2) of these sub-circular polygons outside of the ellipse exhibit green to red coloring, while the interiors (III-3) are green to blue, indicating lower frequency at the boundaries and higher frequency within the polygons. In the western part (T200 to T440, II), the sub-circular morphologies are replaced by linear ones.

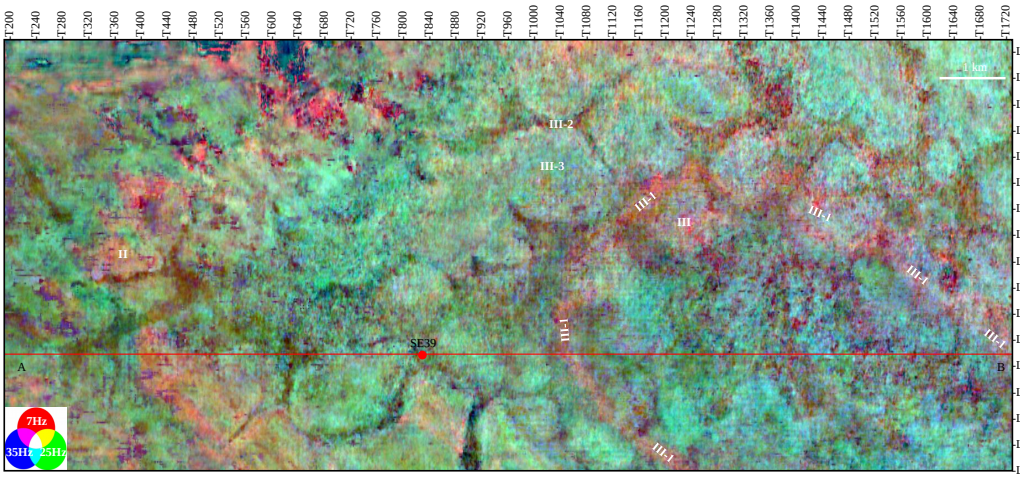

Figure 6. RGB-fused stratal slice 3 at middle K0 in Taidong area, Sanhu Depression, Qaidam Basin (see the green line for the slice location in Figure 2). A-B shows the location of the L130. Letters II, III, III-1, III-2 and III-3 show the locations discussed in the text.

The time-structural maps of the three RGB-fused stratal slices provide valuable insights into the present geomorphology (Figure 7). On the time-structural map of slice 1, the southeastern part (L40 to L300 and T920 to T1720) is a dome dissected by several NNE-SSW ridges (red arrows) and troughs (blue arrows), as seen in Figure 7a. The dome becomes more dispersed due to the cutting of additional troughs and ridges in K1 (Figure 7b). The troughs and ridges are surrounded by relatively sub-circular (e.g., L240 to L290 and T1360 to T1540) and triangular (e.g., L230 to L290 and T1230 to T1350) highs. The ridges narrow,

and the troughs widen on the time-structural map of slice 3 (Figure 7c). The ridges are shown as boundaries around the flat troughs. The relief between the troughs and ridges increases from K2 to K0. The sub-circular geometries formed by troughs and ridges extend to the western part (T200 to T600) in the Taidong area.

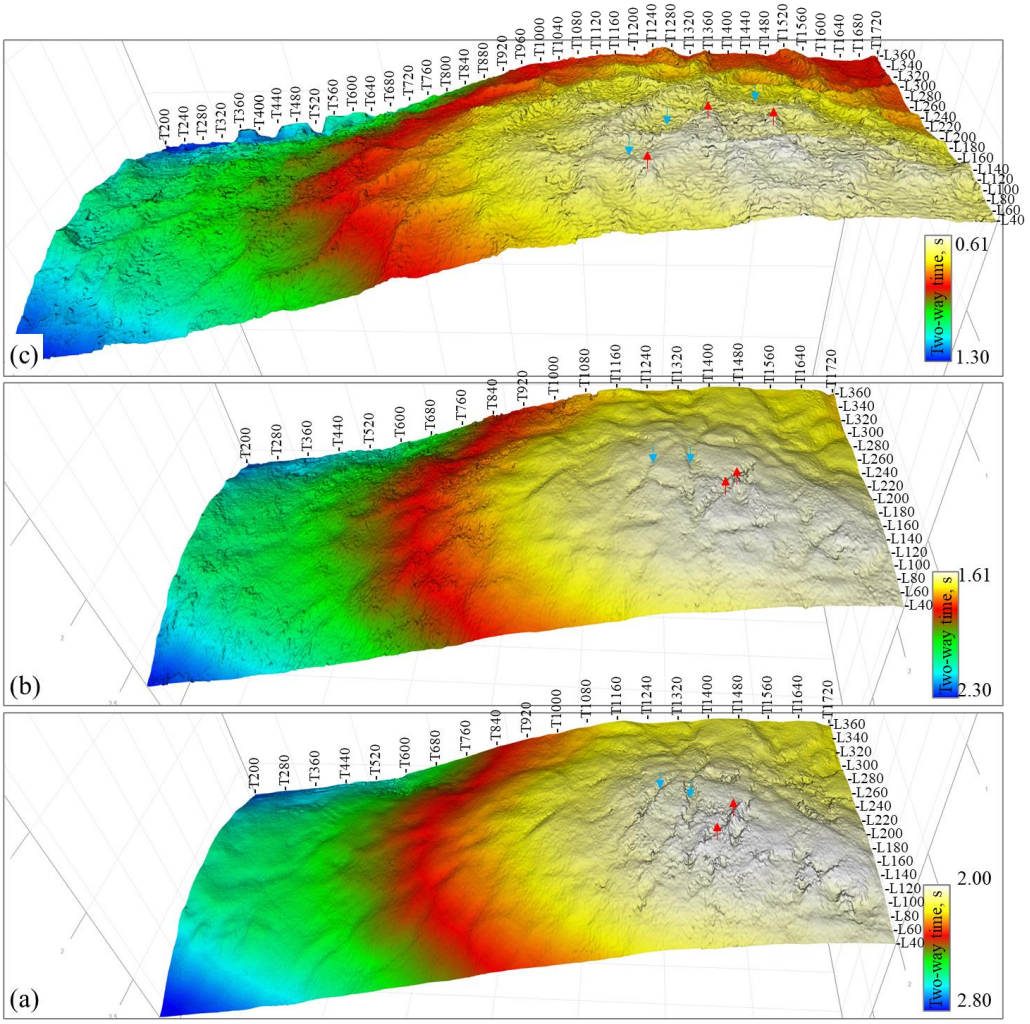

Figure 7. Present time structure maps corresponding to the three stratal slices in K2 (**a**), K1 (**b**), and K0 (**c**) in Taidong area, Sanhu Depression, Qaidam Basin.

The lateral correspondence between geomorphology (time-structural maps) and vertical frequency structure (RGB-fused stratal slices) aids in interpreting the formation mechanisms of the unique linear to sub-circular morphologies observed in the study area. These sub-circular morphologies are present in multiple layers, with their frequency of occurrence increasing from K2 upwards (Figure 8g). Wireline logs also show regular changes. AC (acoustic time logging) generally increases, DEN (Density Logging) decreases, and GR (gamma ray) remain steady with decreasing swing amplitude. The hydrocarbon show during drilling process increases from 5% to around 10%, with a trend of increasing from middle of K1 upwards. Stratal slices 1, 2, and 3, taken from K2, K1, and K0, respectively, were selected as examples to correlate with contemporary regional climate, water salinity, and sedimentary facies.

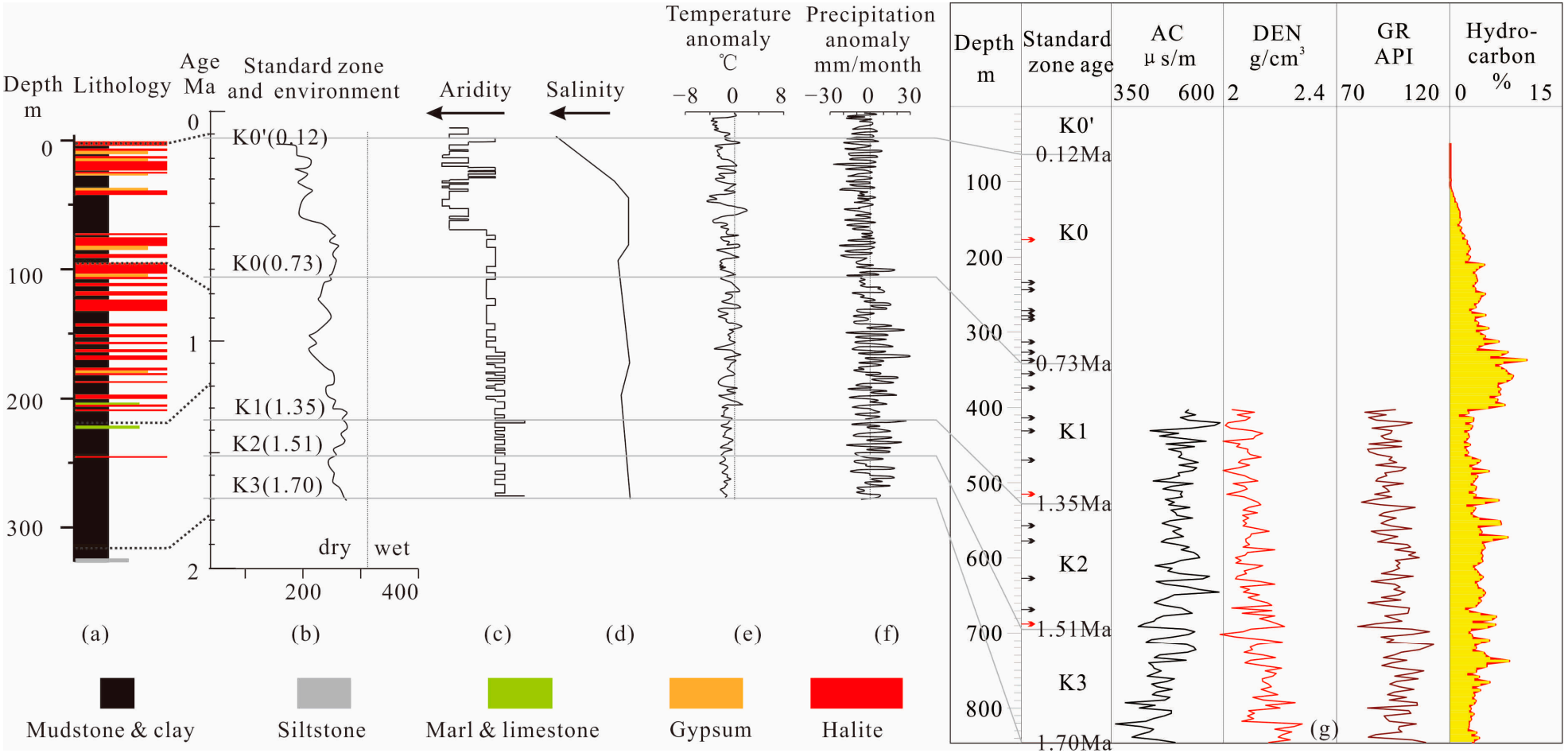

Figure 8. Quaternary regional climate and water salinity in Qaidam Basin and global temperature and precipitation anomaly and well in Taidong area, Sanhu Depression, Qaidam Basin. Lithology in borehole SG-5 [18] (**a**). Mn content and environment in SG-1 and SG-1b [23] (**b**). Water level in SG-1 [30] (**c**). Salinity in SG-1 [31] (**d**). Global temperature anomaly [8,9] (**e**). Global precipitation anomaly [9] (**f**). Well information, wireline logs, hydrocarbon information, and standard zone age [32] in Well SE39 (**g**) (arrows indicate location with sub-circular morphologies; the three red arrows indicate location of the three analyzed slices).

5. Interpretation

Borehole SG-5, located in the western Qaidam Basin, reveals mudstone, clay, siltstone, marl, limestone, gypsum, and halite from a depth of 300 m upwards. Isochronal framework is established according to the age of each standard zones, which connects environment in Taidong area to regional and global paleoclimate. Gypsum and halite begin to appear from around 250 m, corresponding roughly to the K2 standard zone in the Taidong area. The frequency of halite occurrence generally increases as burial depth shallows in the borehole (Figure 8a). Mn concentration data from boreholes SG-1 and SG-1b near SG-5 suggest that the climate has become progressively drier since K3 deposits (~1.7 Ma BP), with two periods of reduced aridity: upper K2 and lower K0 (Figure 8b). Water level and Mg/Ca values in borehole SG-1 were used to reconstruct aridity (Figure 8c) and water salinity (Figure 8d). Both aridity and salinity increased after 1.7 Ma BP, with a sharp escalation occurring after 0.73 Ma BP during K0 deposition. Global temperature anomalies (Figure 8e) and precipitation anomalies (Figure 8f) reflect a continuous decline in both temperature and precipitation, particularly after 0.73 Ma BP. Paleoyardangs found in the Sanhu area at 2.4 Ma BP further indicate persistent hyper-arid conditions since 1.2 Ma BP [33].

Regional climate changes, derived from geological and geochemical data, provide critical insights into interpreting the unique features observed on RGB-fused stratal slices and time-structural maps. The timing and frequency of the sub-circular morphologies align with the evaporite distribution in borehole SG-5 and the regional climate evolution.

Sub-circular morphologies, such as those observed at the Bonneville Salt Flats, Utah [34], generally have much smaller diameters—on the order of several meters—compared to the larger morphologies found in the Taidong area. Therefore, the salt flats in meter-scale with pure saline is not proper to interpret those morphologies in Taidong. Considering geomorphology, vertical-frequency structure, average diameter, and associated lithologies, the sub-circular morphologies in Taidong are interpreted as saline pans formed in an eolian/interdunal sabkha (Figure 9a). This is distinct from sub-circular morphologies found in fluvial-lacustrine (Figure 9b) and marine-dominated sabkhas (Figure 9c) [17,35–37]. Similar sub-circular morphologies with comparable dimensions are also observed in the northeastern region of modern Lake Chad [17], where the saline water is represented in sky-blue, plants in green, and saline sediment in grey-white. Based on observation and previous studies of Lake Chad, the geomorphology features and their evolution are interpreted.

The increase in the restricted degree of water from Lake Chad to its northeastern area follows a distinct pattern (Figure 9a). Freshwater predominates in the open Lake Chad (I), transitioning to semi-restricted brackish water in the northeastern flooded interdunal corridors (II), and finally to restricted brine water in the saline pans of the further northeastern interdunal corridors (III). As salinity increases from west to east, vegetation coverage decreases correspondingly. The water pools exhibit a shift in contour shape, from linear in the flooded interdunal corridors (Figure 10a) to sub-circular in the saline lake (Figure 10b) and the dry saline pan areas (Figure 10c). Linear dunes in the region connect at their ends. The salinity progression across this area starts with fresh water in Lake Chad, moving through brackish and saline water to dry saline pans in the most restricted and evaporite regions.

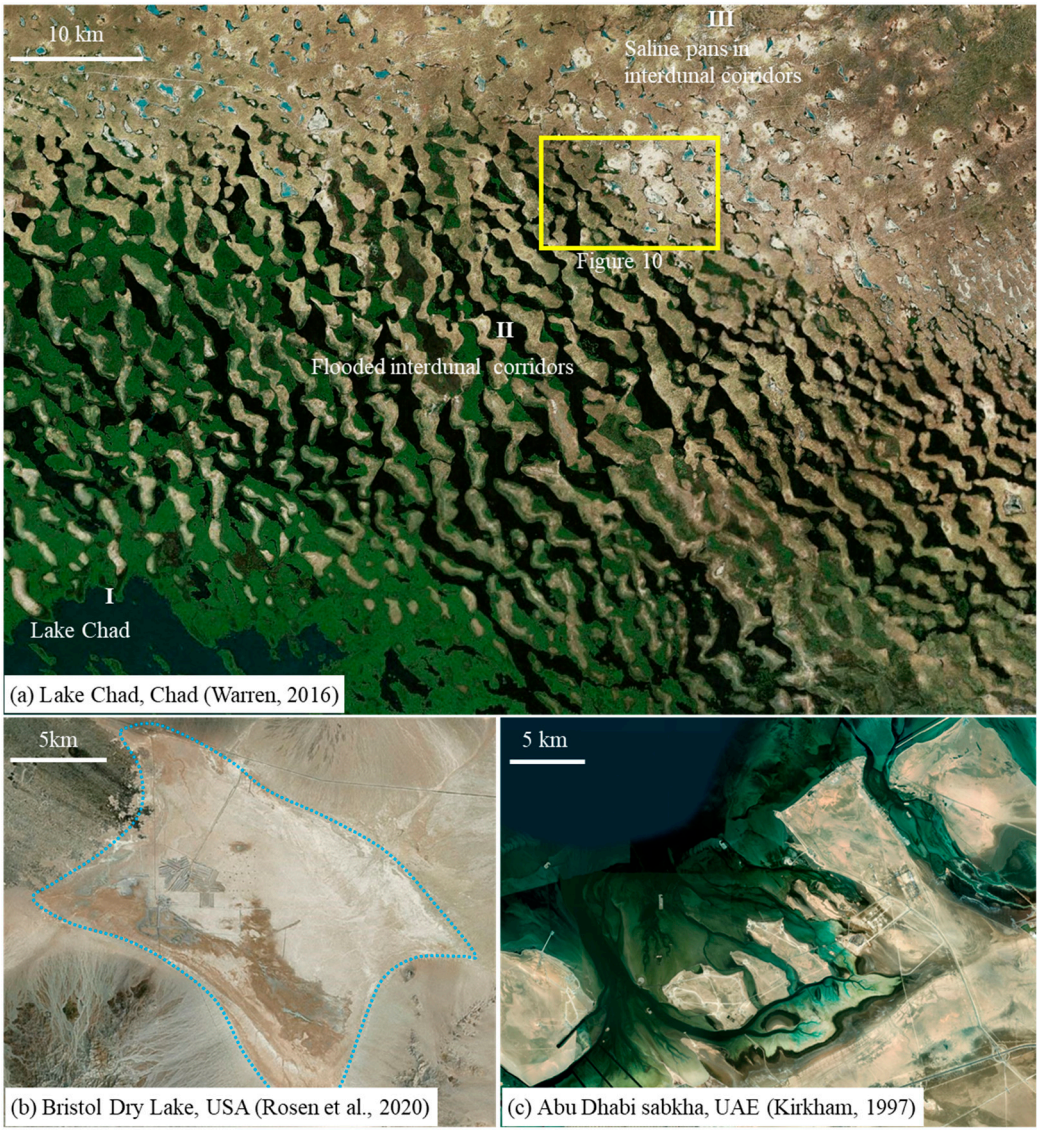

Figure 9. Image of Lake Chad (**a**), Bristol Dry Lake (**b**), and Abu Dhabi sabkha (**c**) to show eolian, fluvial-lacustrine, and marine dominated sabkha, respectively. Warren, 2016 [17]; Rosen, 2020 [37]; Kirkham, 1997 [36].

The sub-circular morphologies in northeastern Lake Chad are driven by monsoonal intensity and consist of dunes and saline pans. Mineral paragenesis in this area follows a sequential pattern from Lake Chad to the beach: calcite, aragonite, magnesium calcite, dolomite, huntite, magnesite, sodium carbonates, sodium sulfates, halite, and sylvite [38]. This lateral mineral distribution changes reflect an increasing degree of evaporation, creating a sedimentary environment dominated by sand and salt deposits. Core analysis reveals a rise in chloride concentration with shallower burial depths [39], indicating a vertical increase in evaporation intensity in the area.

Monsoon winds from the northeast during the dry season and from the southwest during the rainy season govern dune orientation in the region, which typically trends northwest-southeast. In the brackish lakes (Figure 10a) located in the flooded interdunal corridors near Lake Chad, water is semi-restricted with higher salinity than the freshwater of Lake Chad.

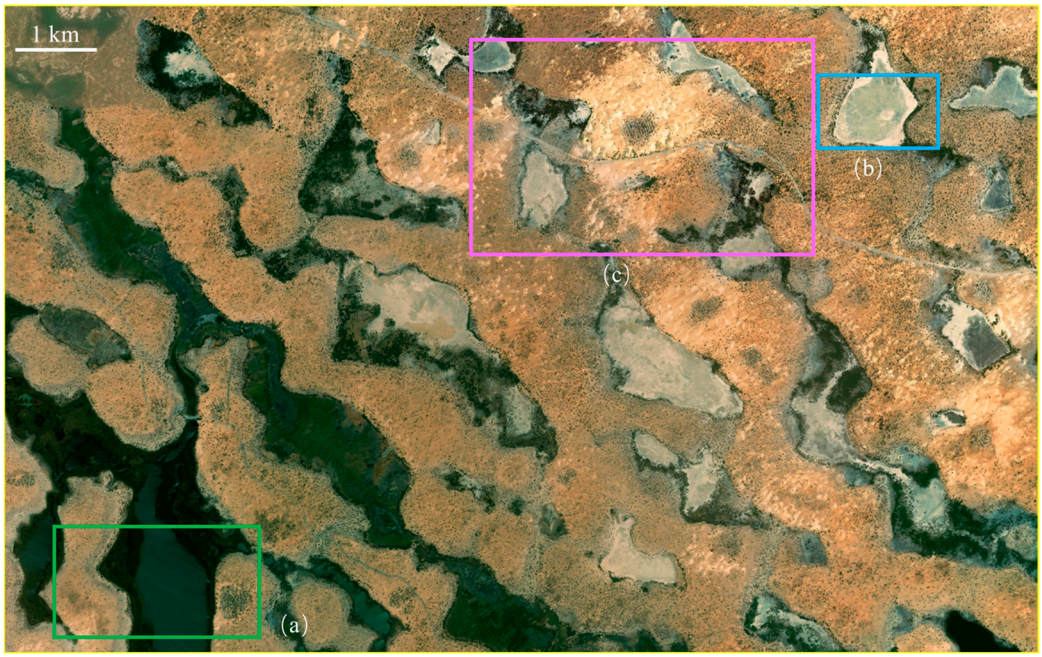

Figure 10. Image of brackish lake (**a**), saline lake (**b**), and dry saline pan (**c**) in interdunal corridors northeastern Lake Chad.

Within the saline lakes, halite and sylvite may precipitate, forming small (tens of meters in diameter) polygonal structures in the southwestern parts of the lake (Figure 11). In the central areas, larger polygons (up to 100 m in diameter) are observed, likely caused by sand bridges or evaporite buildups.

Figure 11. Image of a saline lake in interdunal corridors northeastern Lake Chad.

As evaporation intensifies, a saline lake eventually transforms into a dry saline pan when all brine water evaporates completely (Figure 12). Despite some vegetation planted near a village in the central region, the landscape is almost entirely covered with silt or mixed with evaporite deposits.

Figure 12. Image of a dry saline pan in interdunal corridors northeastern Lake Chad.

Based on the sedimentary environment variations observed in Lake Chad and its northeastern area, we interpret the evaporite facies in Taidong area using the saline pan evolution model proposed by Lowenstein and Hardie [40] (Figure 13a). This model describes the development of saline pans through three key stages: freshwater flooding in a brackish lake, evaporative concentration in a saline lake, and desiccation in a dry saline pan where surface crusts break into sub-circular polygons. In an eolian-dominated setting (e.g., in Lake Chad, Figure 13b), silt can cover these polygons, further influencing the morphology of the sedimentary environment.

Sedimentary process varies in the three stages. During stage 1, the water level is high, and older saline crusts are dissolved by the influx of fresh water. This leads to the deposition of mud and/or eolian silt in the brackish lake. During stage 2, as evaporation intensifies, the water level descents, coincided with saline concentration increases. In the saline lake, subaqueous crystallization occurs, leading to the formation of salt crystals, including syntaxial saline overgrowths and nucleated rafts and hoppers at the water surface. During stage 3, with the completion of the lake water evaporation, a dry saline pan forms. Diagenetic salt growth within the pan and beneath the crust leads to the formation of pressure polygons, exhibiting sub-circular geometries.

In an eolian-dominated sabkha (desert lake), the process continues with ongoing salt growth, fissuring, and dissolution. Eolian silt infiltrates cracks, deforming the crust surface into knobs and ridges. Clays beneath the crust may also be pushed upward through the fractures [41].

Given the generally drying and cooling environmental conditions in the Sanhu area over the past 1.51 million years, an eolian-dominated lacustrine sabkha serves as the geological background for the sedimentary facies observed in the three RGB-fused stratal slices from K2, K1, and K0 in the Taidong area (Figure 13c).

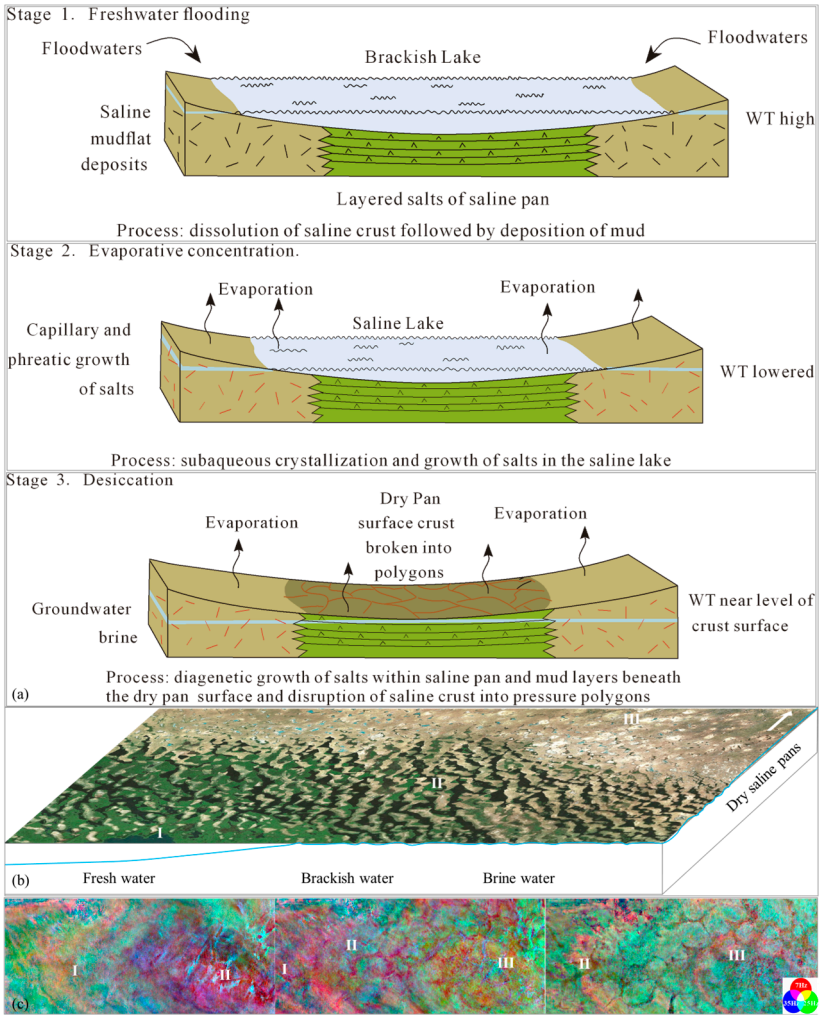

Figure 13. Model of saline pan evolution (**a**) (modified from Lowenstein and Hardie, 1985; Warren, 2016), modern Lake Chad (**b**), and interpretation of evaporite facies in Taidong area, Sanhu Depression, Qaidam Basin (**c**). Letters I to III mark the locations of sedimentary environments from open (I) to semi-restricted (II), and then restricted (III). Colors in subfigure (**c**) indicate the seismic frequency, which can be interpreted as sedimentary facies.

Slice 1 (Figure 13c left): the western part (I) is interpreted as a freshwater lake, while the eastern part (II) is a brackish lake, with embryonic sub-circular geometries in kilometer scale. The orientation of these geometries follows a northeast-southwest trend, nearly vertical to the Quaternary monsoon direction [42] in the Qaidam Basin.

Slice 2 (Figure 13c middle): as evaporation intensifies, the kilometer scale sub-circular geometries become more defined and widespread, indicating a shift to an increasingly evaporite environment. Freshwater lakes retreat to the west (I). Diameter of the subcircular geometries increases slightly in brackish lakes (II) while decreases to less than 1 km in saline lakes (III).

Slice 3 (Figure 13c right): in the final stage of evaporation (K0), dry saline pans (III) emerge in the eastern part of Taidong area. These dry pans are likely covered by eolian silt, which obscures the sub-circular polygons into a larger ellipse with 6.5 km in diameter. The western part (II) remains a saline lake with sub-circular geometries.

Stratal distribution and lithologies observed at the Yanshan outcrop (corresponding to upper Pleistocene), which located at east of the Taidong area, provide further evidence for the evaporite facies interpretation. The strata are gently dipping (<1°) and exhibit parallel interbedding of siltstone (brown), limy-mudstone (light grey), and evaporite saline layers

(greyish-green) at the decimeter scale (Figure 14a). Notably, the evaporite layers contain anhydrite (pink arrow in Figure 14b) and halite (indicated by a green arrow in Figure 14b).

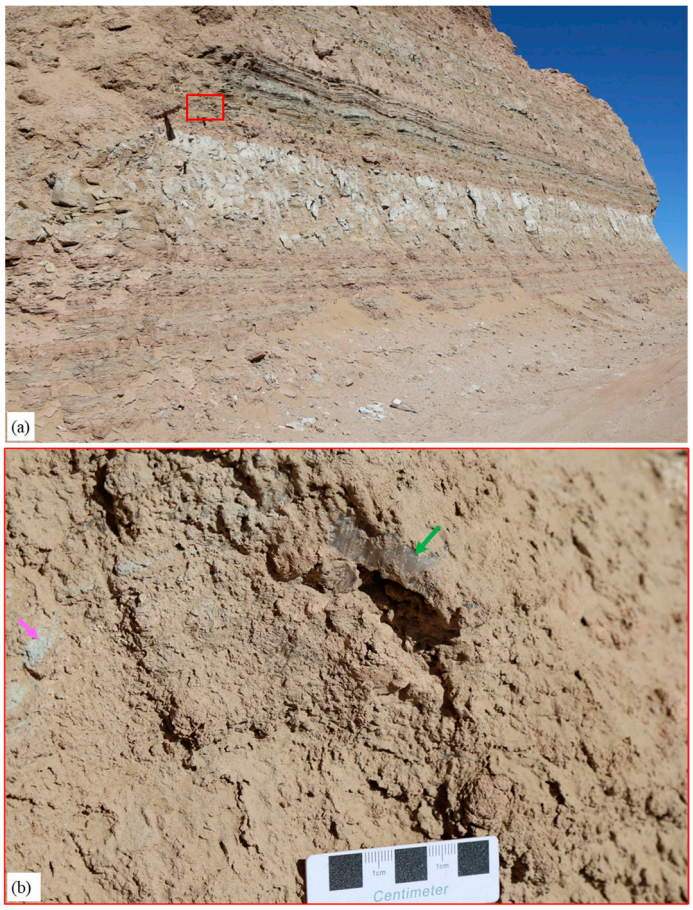

Figure 14. Stratal distribution with a gentle declination (**a**) and evaporites in the strata (**b**) at Upper Pleistocene Yanshan outcrop east of Taidong area, Sanhu Depression, Qaidam Basin. The red square in subfigure (**a**) show the location of subfigure (**b**). The pink and green arrow in subfigure (**b**) point out the location of anhydrite and halite.

6. Conclusions

The S-wave data are unaffected by biogenic gas, and proved to be valuable for constructing the first isochronous framework in the Quaternary biogenic gas-bearing Taidong area in the Sanhu Depression of the Qaidam Basin. By calibrating the S-wave acoustic wireline log, the framework of standard zones interpreted from the seismic data was successfully tied to geological ages.

Seismic sedimentological techniques—such as phase rotation, frequency decomposition, RGB fusing, and stratal slicing—are proved effective in mapping facies at different depths from K2 upward across the Taidong area. By integrating regional climate data, water salinity information, lithologies of outcrop and borehole samples, and modern analogs, seismic sedimentology slices were comprehensively interpretated to be sedimentary facies based on their geomorphological and frequency characteristics.

The sub-circular polygons recognized on the stratal slices generated by seismic sedimentology were interpreted as evaporite facies, i.e., brackish lake, brine saline lake, and dry saline pans for the first time in Taidong area. The evaporite facies in Taidong area occur from K2 (1.51 Ma BP) and increase in frequency thereafter. The evaporite intensity generally increased in response to regional rises in aridity and water salinity. Spatial variation of different evaporite environments is identified, with fresh water lakes in the west, brack-

ish lakes in the middle, and brine saline lakes and/or dry saline pans covered by silt in the east.

The lateral distribution and vertical evolution of evaporite facies in the Taidong area provide critical insights into the hydrological changes related to regional climates during the Quaternary period. The outcomes of this study not only assist in identifying optimal sealing rocks for biogenic gas accumulation but also provide valuable locations for the exploration and extraction of evaporite resources in the region.

Author Contributions: Conceptualization, G.L. and Z.X.; methodology, G.L., Z.X., H.Z. and X.Z.; validation, Z.X. and Y.S.; formal analysis, J.L. and C.L.; investigation, G.L., Z.X., J.L., C.L., J.T. and L.J.; resources, G.L., Z.X., J.L., C.L. and J.T.; writing—original draft preparation, Z.X. and G.L.; writing—review and editing, G.L., H.Z., Y.S. and X.Z.; funding acquisition, Z.X. All authors have read and agreed to the published version of the manuscript.

Funding: This research was funded by National Science and Technology Major Project of China, grant number 2024ZD1003307; PetroChina Science and Technology Projects, grant numbers 2022-N/G-47808, 2023-N/G-67014, and 101023hx0001b93001; International Cooperation Projects between PetroChina Research Institute of Petroleum Exploration & Development and The University of Texas at Austin, grant numbers 15HT10500000010 and 19HTY5000008.

Institutional Review Board Statement: Not applicable.

Informed Consent Statement: Not applicable.

Data Availability Statement: Embargo on data due to commercial restrictions.

Conflicts of Interest: Authors Guoyong Liu, Zhaohui Xu and Jiangtao Li were employed by PetroChina Qinghai Oilfield Company. The remaining authors declare that the research was conducted in the absence of any commercial or financial relationships that could be construed as a potential conflict of interest.

References

1. George, E.C.; Charles, N.T.; Leslie, B.M. Biogenic and thermogenic origins of natural gas in Cook Inlet Basin, Alaska. *AAPG Bull.* **1980**, *64*, 1131–1139.
2. John, D.G.; George, F.H. Giant gas fields of northern west Siberia. *AAPG Bull.* **1986**, *70*, 830–852.
3. Czauner, B.; Szabó, Z.; Márton, B.; Mádl-Szőnyi, J. Basin-scale hydraulic evaluation of groundwater flow controlled biogenic gas migration and accumulation in the central Pannonian Basin. *Water* **2023**, *15*, 3272. [CrossRef]
4. Efrina, C.A.P.; Hermes, P.; Hamriani, R.; Nor, S.H. Biogenic gas—"From drilling hazard to promising future hydrocarbon resource": Study of Mamberamo Frontier Basin, north Papua, Indonesia. *BIO Web Conf.* **2023**, *73*, 04007.
5. Dudley, D.R.; George, E.C. Generation, accumulation, and resource potential of biogenic gas. *AAPG Bull.* **1981**, *65*, 5–25.
6. Xu, Z.; Li, J.; Li, J.; Chen, Y.; Yang, S.; Wang, Y.; Shao, Z. Application of 9-component S-wave 3D seismic data to study sedimentary facies and reservoirs in a biogas-bearing area: A case study on the Pleistocene Qigequan Formation in Taidong area, Sanhu Depression, Qaidam Basin, NW China. *Petrol. Explor. Develop.* **2024**, *51*, 647–660. [CrossRef]
7. Li, Y.; Lin, C. Exploration methods for late Quaternary shallow biogenic gas reservoirs in the Hangzhou Bay area, eastern China. *AAPG Bull.* **2010**, *94*, 1741–1759. [CrossRef]
8. Wara, M.W.; Ravelo, A.C.; Delaney, M.L. Permanent El Niño-Like conditions during the Pliocene warm period. *Science* **2005**, *309*, 758–761. [CrossRef] [PubMed]
9. Williams, C.J.R.; Lord., N.S.; Kennedy-Asser, A.T.; Richards, D.A.; Crucifix, M.; Kontula, A.; Thorne, M.; Valdes, P.J.; Foster, G.L.; Brown, R.; et al. The relative role of orbital forcing, CO_2 and ice sheet feedbacks on Quaternary climate. *Res. Sq.* **2024**, *preprint*.
10. Goldsmith, L.H. Concentration of potash salts in saline basins. *AAPG Bull.* **1969**, *53*, 790–797.
11. Sirota, I.; Enzel, Y.; Lensky, N. Halite focusing and amplification of salt thickness: From the Dead Sea to deep hypersaline basins. *Geology* **2018**, *46*, 851–854. [CrossRef]
12. Morris, R.C.; Dickey, P.A. Modern evaporite deposition in Peru. *AAPG Bull.* **1957**, *41*, 2467–2474.
13. Milewski, R. Potential of Optical Remote Sensing for the Analysis of Salt Pan Environments. Ph.D. Thesis, University of Potsdam, Potsdam, Germany, 2020.

14. Teixeira, L.; Lupinacci, W.; Maul, A. Quantitative seismic-stratigraphic interpretation of the evaporite sequence in the Santos Basin. *Mar. Pet. Geol.* **2020**, *122*, 104690. [CrossRef]
15. Deng, Z.W.; Zhang, R.; Gou, L.; Zhang, S.H.; Yue, Y.Y.; Chang, X.J.; Wu, Y.G.; Wang, Y.; Ni, Y.D.; Yan, Z.H.; et al. Direct shear-wave seismic survey in Sanhu area, Qaidam Basin, west China. *Lead. Edge* **2022**, *41*, 47–53. [CrossRef]
16. Goodall, T.M.; North, C.P.; Glennie, K.W. Surface and subsurface sedimentary structures produced by salt crusts. *Sedimentology* **2000**, *47*, 99–118. [CrossRef]
17. Warren, J.K. *Evaporites: A Geological Compendium*, 2nd ed.; Springer International Publishing Switzerland: Cham, Switzerland, 2016; p. 1813.
18. Zhang, W.; Li, T.; Fang, X.; Zhang, T.; Yan, M.; Zan, J.; Yang, Y.; Khatri, D.B. Chronological and rock magnetic constraints on the transition of the Quaternary paleoclimate in the western Qaidam Basin, NE Tibetan Plateau. *Quat. Res.* **2021**, *104*, 170–181. [CrossRef]
19. Jin, Z.; Zhang, M.; Tang, L.; Li, J. Evolution of Meso-Cenozoic Qaidam Basin and its control on oil and gas. *Oil Gas Geol.* **2004**, *25*, 603–608.
20. Manabe, S.; Broccoli, A.J. Mountains and arid climates of middle latitudes. *Science* **1990**, *247*, 192–195. [CrossRef]
21. Shao, Z.; He, S.; Hou, L.; Wang, Y.; Tian, C.; Liu, X.; Zhou, Y.; Hao, M.; Lin, C. Dynamic accumulation of the Quaternary shale biogas in Sanhu Area of the Qaidam Basin, China. *Energies* **2022**, *15*, 4593. [CrossRef]
22. Liu, X.X.; Jiang, Z.X.; Tang, X.L.; Zhu, J.; Zhang, F.Y.; Wang, Y.C.; Xu, M.S. Geochemical characteristics and origin of the formation water of the Saline Lake Basin: A case study of the Quaternary Qigequan Formation in the Sanhu Depression, Qaidam Basin. *Geosci. Lett.* **2024**, *11*, 1–13. [CrossRef]
23. Liu, Y.; Yang, Y.; Ye, C.; Yang, R.; Appel, E.; Fang, X. Global change modulated Asian inland climate since 7.3Ma: Carbonate manganese records in the western Qaidam Basin. *Front. Earth Sci.* **2021**, *9*, 813727. [CrossRef]
24. Zeng, H.; Henry, S.C.; Riola, J.P. Stratal slicing: Part II. Real seismic data. *Geophysics* **1998**, *63*, 514–522. [CrossRef]
25. Zeng, H.; Hentz, T.F. High-frequency sequence stratigraphy from seismic sedimentology: Applied to Miocene, Vermilion Block 50, Tiger Shoal area, offshore Louisiana. *AAPG Bull.* **2004**, *88*, 153–174. [CrossRef]
26. Zeng, H.; Zhao, W.; Xu, Z.; Fu, Q.; Hu, S.; Wang, Z.; Li, B. Carbonate seismic sedimentology: A case study of Cambrian Longwangmiao Formation, Gaoshiti-Moxi area, Sichuan Basin, China. *Petrol. Explor. Dev.* **2018**, *45*, 830–839. [CrossRef]
27. Kallweit, R.S.; Wood, L.C. The limits of resolution of zero-phase wavelets. *Geophysics* **1982**, *47*, 1035. [CrossRef]
28. Henderson, J.; Purves, S.J.; Fisher, G.; Leppard, C. Delineation of geological elements from seismic attributes and RGB blending. *Lead. Edge* **2008**, *27*, 342–350. [CrossRef]
29. Xu, Z.; Hu, S.; Wang, L.; Zhao, W.; Cao, Z.; Wang, R.; Shi, S.; Jiang, L. Seismic sedimentologic study of facies and reservoir in middle Triassic Karamay Formation of the Mahu Sag, Junggar Basin, China. *Mar. Pet. Geol.* **2019**, *107*, 222–236. [CrossRef]
30. Wang, J.; Fang, X.; Appel, E.; Song, C. Pliocene-Pleistocene climate change at the NE Tibetan Plateau deduced from lithofacies variation in the drill core SG-1, western Qaidam Basin, China. *J. Sediment. Res.* **2012**, *82*, 933–952. [CrossRef]
31. Lu, S.; Ma, Y.; Lü, S.; Han, W.; Han, S.; Han, F.; Fang, X. Systematic boron isotope analysis on a Quaternary deep SG-1 core from the Qaidam Basin, NE Tibetan Plateau and its paleoclimate implication. *Quat. Int.* **2022**, *631*, 1–10. [CrossRef]
32. Liu, Z.; Sun, S.; Yang, F.; Zhou, Z. Quaternary stratigraphy and its chronology analysis from Sanhu region of Qaidam Basin. *Sci. China (Ser. B)* **1990**, *11*, 1201–1212.
33. Heermance, R.V.; Pullen, A.; Kapp, P.; Garzione, C.N.; Bogue, S.; Ding, L.; Song, P. Climatic and tectonic controls on sedimentation and erosion during the Pliocene-Quaternary in the Qaidam Basin (China). *GSA Bull.* **2013**, *125*, 833–856. [CrossRef]
34. Bowen, B.B.; Kipnis, E.L.; Raming, L.W. Temporal dynamics of flooding, evaporation, and desiccation cycles and observations of salt crust area change at the Bonneville Salt Flats, Utah. *Geomorphology* **2017**, *299*, 1–11. [CrossRef]
35. Hanford, C.R. A process-sedimentary framework for characterizing recent and ancient sabkhas. *Sediment. Geol.* **1981**, *30*, 255–265. [CrossRef]
36. Kirkham, A. Shoreline Evolution, Aeolian deflation and anhydrite distribution of the Holocene, Abu Dhabi. *GeoArabia* **1997**, *2*, 403–416. [CrossRef]
37. Rosen, M.R.; Stillings, L.L.; Kane, T.; Campbell, K.; Vitale, M.P.G.; Spanjers, R.P.G. Li and Ca enrichment in the Bristol dry lake brine compared to brines from Cadiz and Danby dry lakes, Barstow-Bristol Trough, California, USA. *Minerals* **2020**, *10*, 284. [CrossRef]
38. Gac, J.Y.; Al-Droubi, A.; Paquet, H.; Fritz, B.; Tardy, Y. Chemical model for origin and distribution of elements in salts and brines during evaporation of waters. Application to some saline lakes of Tibesti, Chad. *Phys. Chem. Earth* **1979**, *11*, 149–158. [CrossRef]
39. Isiorho, S.A.; Matisoff, G.; Wehn, K.S. Seepage relationships between Lake Chad and the Chad aquifers. *Ground Water* **1996**, *34*, 819–826. [CrossRef]
40. Lowenstein, T.K.; Hardie, L.A. Criteria for the recognition of salt-pan evaporites. *Sedimentology* **1985**, *32*, 627–644. [CrossRef]

41. Lugli, S.; Schreiber, B.C.; Triberti, B. Giant polygons in the Realmonte mine (Agrigento, Sicily): Evidence for the desiccation of a Messinian halite basin. *J. Sediment. Res. Sect. A-Sediment. Petrol. Process.* **1999**, *69*, 764–771. [CrossRef]
42. Ma, F.; Lv, P.; Cao, M. The effects of wind regime and sand supply on the coexistence of barchans and linear dunes in China's Qaidam Basin. *Front. Earth Sci.* **2022**, *10*, 897640. [CrossRef]